Particle & Particle Systems Characterization
www.particle-journal.com

Aerosol Synthesis and Reactivity of Thin Oxide Shell Aluminum Nanoparticles via Fluorocarboxylic Acid Functional Coating

*Daniel A. Kaplowitz, Guoqiang Jian, Karen Gaskell, Aldo Ponce, Panju Shang, and Michael R. Zachariah**

There is currently a need for low oxide content nanoaluminum as a component in high-energy-density fuels. A gas-phase passivation coating of perfluoropentanoic acid on in situ generated bare nanoaluminum accomplished in an aerosol stream and resulting in an air-stable product is demonstrated. Transmission electron microscopy inspection demonstrates a 1–2 nm coating layer, and thermogravimetric analysis reveals an 80% active fuel content, an increase of 17% from untreated product. X-ray photoelectron spectroscopy confirms both the presence of the fluorocarboxylic acid on the aluminum surface and the thinner coating layer compared with the untreated case. A bridge bonding coordination between the carboxylate group and aluminum is indicated via Fourier transform infrared spectroscopy. The coated product demonstrates reduced ignition temperature in thermite combinations for temperature-jump fine wire combustion tests and X-ray photoelectron spectroscopy verifies formation of AlF_3 in burned product.

1. Introduction

The high energy content of metal/oxidizer combinations compared with CHNO-based materials has motivated considerable investigation in their energetic applications requiring rapid energy release.[1–3] Reactive metals can have an extremely high energy density, but performance is hindered by diffusion-limited kinetics between oxidizer and metal. By decreasing particle size to the nanoscale, a substantial increase in surface to volume ratio of the metal particle can substantially improve reaction rate. For energetic formulations in the nanoregime, aluminum is the leading fuel component due to its ready availability and reactivity.[4–6] While many different nanoscale oxidizers are employed, aluminum is a main focus. A major concern with production and use of nanoaluminum is the native oxide that naturally forms when any bare aluminum is exposed to air. For micrometer-sized aluminum particles, this 3–5 nm oxide layer accounts for only a small fraction of the particle mass. For nanosized aluminum, however, this oxide coating can represent a large fraction of the particle's mass. A 50-nm particle with a 5-nm alumina shell will contain 58% of the particle's total mass as aluminum oxide, leaving a much smaller amount of material available for an energetic process. The other concern with this alumina layer is its significant impedance to reaction due to its poor reactivity and high melting point of 2072 °C compared to aluminum's 660 °C. For further reaction between aluminum and oxygen, the core material must either escape the shell or oxidizer must diffuse through.[7,8] In this study, we focus on an approach to form a different layer that will enhance aluminum transport and reactivity.

Developing a coating before oxidation can occur is the most common technique to prevent surface oxidation of aluminum.[9–13] Such a passivation layer can be used for storage and be removed when the aluminum is needed. A nonpyrophoric unpassivated nanoaluminum was prepared by Hammertroem et al.[9] by polymerizing epoxides on the particle surface in solution. A functional energetic material coating that can directly react with the aluminum core during combustion, however, can prove to be a more valuable application. This functional coating on bare aluminum would not only prevent the oxide layer from forming but also affect agglomeration during processing and alter the energy release mechanisms during combustion. If an oxidizer is attached directly to the aluminum surface while preventing a spontaneous run-away reaction, the resulting structure will have higher energy content with the potential of favorably altered kinetics.

Jouet et al.[10] were able to successfully prevent oxidation of nanoaluminum by forming a self-assembled monolayer (SAM) of a perfluorotetradecanoic acid ($C_{14}HF_{27}O_2$) on the particle surface in solution, thus functionalizing the surface to enhance reactivity. Subsequent shock reactivity testing of

Dr. D. A. Kaplowitz, G. Jian, Dr. P. Shang,
Prof. M. R. Zachariah
Department of Chemical and Biomolecular Engineering
University of Maryland
College Park, MD 20742, USA
E-mail: mrz@umd.edu
Dr. K. Gaskell, Dr. A. Ponce
Department of Chemistry and Biochemistry
University of Maryland
College Park, MD 20742, USA

DOI: 10.1002/ppsc.201300112

the product combined with organic high explosives shows a significant enhancement compared with conventional Al, and laser ignition experiments show fast reaction capacities for the passivated product.[11] Horn et al.[14] prepared similar perfluorocarboxylic acid coatings on nanoaluminum particles that had already formed an oxide layer. This product in thermite combinations demonstrated via flame tests that even without passivation, energetic improvement can still be achieved from direct oxidizer delivery in a nanoparticle coating.[15]

Fluorination of aluminum to produce AlF_3 can produce a significant increase in energy release, 56 kJ g^{-1} of aluminum, compared with formation of Al_2O_3, which releases 31 kJ g^{-1}.[14] The stoichiometric exothermic reaction of aluminum with fluorocarbon will produce AlF_3 and carbon according to the reaction shown in Equation (1).[16]

$$2Al + 3(-CF_2-)_n \rightarrow 3C + 2AlF_3 \quad \Delta H^0 = -591.98\,kJ \qquad (1)$$

Teflon has been heavily focused on for studies involving fluorination of aluminum. Watson et al.[17] examined combustion reactions for aluminum/Teflon compared with aluminum/MoO_3 combinations for closed and open configurations, concluding that for closed system combustion, fluorine oxidizing combinations can yield increased heat of combustion and gas generation compared with the metal oxide. For open-system combustion, however, they found that the higher gas generation can hinder the reaction due to loss of the liberated gas.

Further investigation into the mechanism for interaction between fluorine and aluminum was undertaken by Pantoya and Dean,[18] probing a preignition reaction between aluminum oxide and fluorine. DSC–TGA experiments for aluminum oxide nanoparticles combined with Teflon showed a significant exotherm starting at 400 °C, indicating fluorination of aluminum oxide. This suggests that not only can fluorocarbon combinations with aluminum metal powder provide increased energy release, an early fluorine reaction with an aluminum oxide layer could change the combustion reaction mechanism, avoiding issues with the poor reactivity and high melting point of the aluminum oxide shell.

Commercial nanoaluminum already necessarily has a native oxide coating, so we need to create nanoaluminum in a non-oxidizing environment, and then proceed to passivate the particle on-the-fly. Previous work yielded a low-temperature gas-phase scheme using triisobutylaluminum (TibAl) as a metal organic precursor, which decomposed in the gas phase at 350 °C produces an aerosol of highly faceted crystals of aluminum.[19] Particles grow into a polyhedral morphology with an average diagonal distance of ≈90 nm. Production was accomplished under argon gas, thus allowing formation of a bare aluminum surface. The in-line aerosol process lends itself well to combination with coating systems for passivation. Without such a coating, the exposed aluminum forms a 4-nm oxide layer.

For an organic passivation coating on aluminum, several options were available. In the nano-regime, the epoxide polymerization technique on aluminum in solution has been demonstrated to be a very successful method for capping and stabilization of aluminum.[9] Though valuable, this method does not translate well to a gas-phase coating system due to the multiple step reactions needed to polymerize. For an aerosol-produced organic passivation layer, simple techniques with waxes or carbon chain materials could prove fruitful due to their ease of incorporation into a bubbler system. A paraffin wax technique was explored for protection of titanium oxide particles by Balasubramanian et al.[12] In a similar method, stearic acid was successfully deposited on the surface of silver nanoparticles for protection in an evaporation system by Zhang et al.[13] Information from these experiments was incorporated into bubbler techniques for coating of aluminum to allow fine-tuned flow control of coating material. These materials, however, would only potentially provide enhancement due to prevention of aluminum oxidation.[9]

For a functional coating to enhance oxidizer delivery, the use of perfluorocarboxylic acids, though still accomplished in solution, shows potential for development in an aerosol system.[10] The carboxylic acid group on the end of the fluorocarbon chain should preferentially react with the bare aluminum surface, forming a SAM for protection from penetration of oxygen. Several perfluorocarboxylic acids were investigated for coating production, but perfluoropentanoic acid (PFPA; $C_5HF_9O_2$) was ultimately chosen for functionalized passivation as its liquid phase at room temperature and relatively low boiling point of 140 °C allow for ease of incorporation into a bubbler system for gas-phase coating.

In this work, we develop an aerosol-based approach for in-line perfluorocarboxylic acid passivation of synthesized bare nanoaluminum. Coating the core material as it is produced avoids potential scale up concerns with passivation processing of batch samples in oxygen-free atmospheres. We will demonstrate that under appropriate conditions, gaseous PFPA treatment of bare nanoaluminum can produce a SAM that protects the metallic core from thick aluminum oxide layer formation. This material is then tested for reactivity relative to untreated product, indicating extremely high active fuel content and reduced critical ignition temperature for CuO thermite combinations.

2. Experimental Section

2.1. Aerosol Synthesis of Perfluoropentanoic Acid-Coated Nanoaluminum

The basic experimental configuration is shown in **Figure 1**. The bare aluminum production technique developed previously[19] involves bubbling of argon through 60 °C heated triisobutylaluminum precursor with a partial pressure of 3.3 mmHg and subsequent thermal pyrolysis at 350 °C in a total flow of 3000 sccm. This aerosol product, consisting of an aluminum total mass flow of 13 mg min^{-1}, was sent to the gas-phase coating section employing a glass bubbler containing 25 mL of PFPA heated to 80 °C with an Omegalux heating tape connected to a variable transformer. The outlet stream from the bubbler contained the aluminum aerosol flow in a PFPA mass concentration of 10.3 μg cm^{-3} sent via high-temperature-resistant tubing 20 in. in length for collection on Sterlitech 0.2 μm polytetrafluoroethylene membrane disc filters. To accomplish a gas-phase reaction, the coating zone at the outlet of the PFPA bubbler was heated to 170 °C, above the boiling point of PFPA (140 °C), to ensure all of the coating material remained in the gaseous state. The collection filter was heated to this temperature, as well, to ensure the only acid collected in

DOI: 10.1002/ppsc.201300112

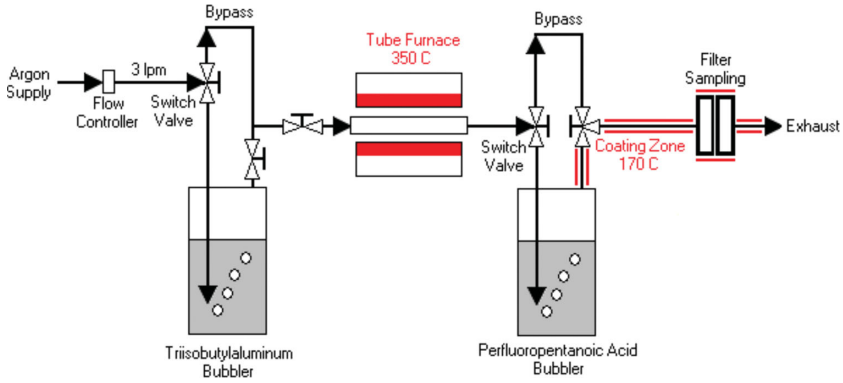

Figure 1. Experimental setup for perfluoropentanoic acid coating of Al.

the product will be the fluorocarbon chains bound to the bare aluminum surface, thus forming a SAM.

2.2. High-Resolution Transmission Electron Microscopy (HRTEM)

The collected sample was deposited on carbon film 200 mesh copper grids from Electron Microscopy Sciences for HRTEM imaging (JEOL JEM 2100FE-TEM) with a focus on the particle edge in order to evaluate coating thickness.

2.3. Fourier Transform Infrared (FTIR) Spectroscopy

Infrared spectra were obtained using the Thermo Nicolet Nexus 670 FTIR utilizing a highly sensitive MCT detector with CaF_2 crystals for sample containment within a nitrogen atmosphere.

2.4. Thermogravimetric Analysis (TGA)

A TA Instruments Q500 thermogravimetric analyzer was employed using a quartz crucible for sample containment. The heating event consisted of a 10 °C min^{-1} ramp to 1200 °C and a hold for 30 min at 1200 °C with weight measurements recorded every 0.5 s.

2.5. X-Ray Photoelectron Spectroscopy Characterization

Samples were inspected with the Kratos AXIS 165 spectrometer operated in hybrid mode and excited with monochromated aluminum X-rays at 280 W in an ultra-high vacuum chamber with a base pressure $\leq 5 \times 10^{-8}$ Torr. Charge neutralization was required to minimize surface charge buildup, all spectra were referenced to C1s at 284.8 eV, and the background was subtracted by Shirley's method.

2.6. Wire Temperature-Jump Ignition and High-Speed Video

Ignition temperatures in air of fuel product samples in stoichiometric thermite combination with CuO nanoparticles (<50 nm; Sigma–Aldrich) were measured after sonication in hexane for 30 min, the sample was deposited on a 76-μm diameter platinum wire with a total heated length of ≈12 mm that was replaced after each heating test, as detailed by Zhou et al.[20] Combustion was initiated by connecting the wire to a high-voltage power source varied by changing the pulse voltage, resulting in heating rates of $\approx 4 \times 10^5$ Ks^{-1}. A Phantom V12 high-speed digital camera monitored the combustion behavior of the nanothermite on the wire. Measurements were recorded for voltage and transient current through the circuit, and wire resistance measurements allowed for real-time temperature information throughout the event.

3. Results and Discussion

3.1. Product Inspection

Inspection of HRTEM images shown in **Figure 2**a reveals a thin layer coating at the edge of the aluminum particle treated by PFPA, ranging from 1 to 2 nm, a significant difference from

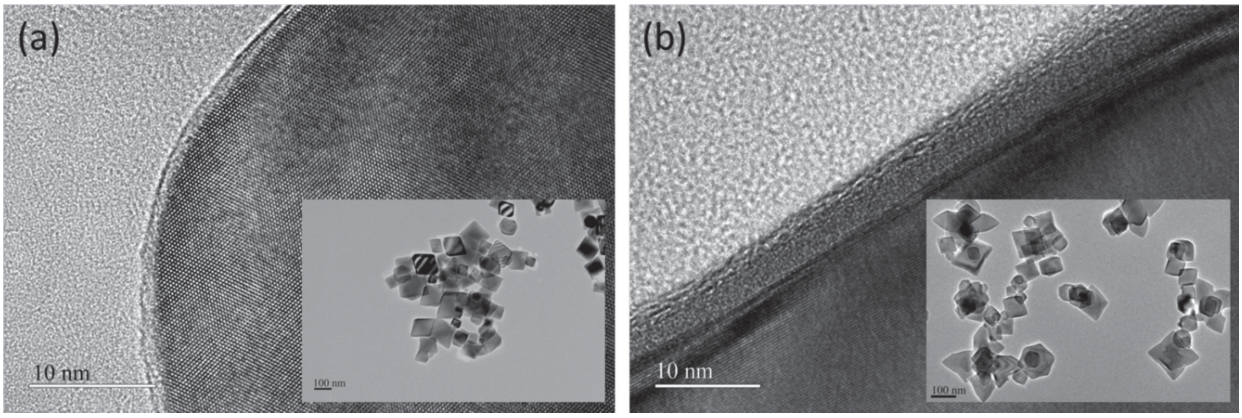

Figure 2. High-resolution TEM images of nanoaluminum a) PFPA treated and b) untreated. Note: insets are lower magnification TEM images of product.

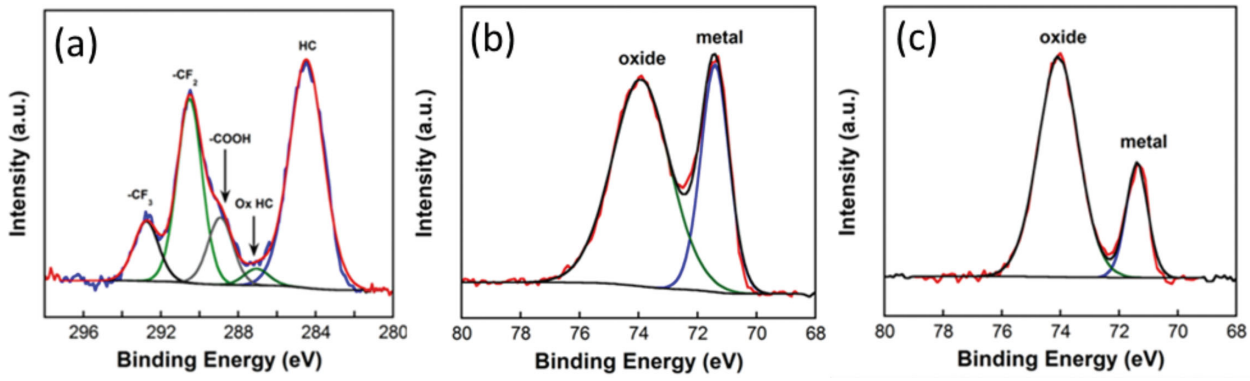

Figure 3. XPS spectra for product a) C1s PFPA treated, b) Al2p PFPA treated, and c) Al2p untreated.

the regular ≈4 nm aluminum oxide layer from the untreated case in Figure 2b. The particle product is air stable and does not show any indication of reaction or degradation upon air exposure or storage under standard atmospheric conditions.

The coated product shows an aluminum core structure identical to previous untreated results yielding single crystalline particles of polyhedral shape. The phase of aluminum is confirmed by lattice spacing measurements of 0.229 nm consistent with a literature value of 0.233 nm.[19]

XPS spectra will give local composition characterization of the edge of these particles by analysis of electrons expelled from the top 1 to 10 nm of the particle during irradiation, with this penetration distance largely depending on the density of the material. Results are fit and shown in **Figure 3** to analyze the presence of the fluorocarbon in the C1s spectrum for the treated sample, detect the presence of aluminum oxide bonding in Al2p, and compare penetration distance into the metal core for treated and untreated aluminum.

Figure 3a demonstrates that fluorocarbon is indeed present at the surface of the particle, indicated by the presence of CF_2, CF_3, and COOH groups. The remaining peaks are attributed to expected hydrocarbon and oxidized hydrocarbon contamination accumulated on the product. Since the collection filter for the coated product is kept above the boiling point of the PFPA, we can be sure that all perfluorocarboxylic acid chains are bound to the aluminum surface. To evaluate the aluminum bonding at particle edge, XPS spectra calibrated to Al2p at 71.4 eV are shown in Figure 3b,c comparing PFPA-treated aluminum to untreated, respectively.

Inspection of these results shows a significantly higher aluminum metal peak for the PFPA-treated product in relation to the oxide. For the untreated case in Figure 3c, the ≈4 nm aluminum oxide layer yields an XPS peak with a much higher intensity than that of the pure aluminum metal. Figure 3b, however, shows a contrasting result; the aluminum metal peak is higher than that of the oxide. XPS has probed further into the core aluminum than in the untreated case, confirming TEM observations of a significantly thinner coating layer. Additionally, the oxide peak in Figure 3b is not entirely attributed to formation of Al_2O_3. In this spectrum, aluminum oxide cannot easily be distinguished from the aluminum bound to oxygen atoms in the carboxylic acid group of the fluorocarbon chain. To analyze the percentage of aluminum oxide formed with relation to functionalized aluminum, the bonding arrangement between the carboxylate groups in the PFPA coating must be analyzed.

There are three potential arrangements for bonding between aluminum and the carboxylic acid group: monodentate coordination involves a single oxygen atom bonding to aluminum while one remains disengaged, bidentate has both oxygen atoms bound to one single aluminum atom, and bridging has each oxygen atom binding to separate aluminum atoms at the surface. Jouet et al.[10] found by FTIR examination appropriate frequencies indicating perfluorotetradecanoic acid will adopt the bridging structure. Since our coating layer is composed of a different fluorocarboxylic acid, we use FTIR to investigate if this treatment has formed a similar bonding structure. Resulting transmittance plots are shown in **Figure 4**, and peaks are fitted based on accepted band assignments.[21]

Spectra show the change in bonding for the carboxylate group on PFPA. Peaks for ν_a(COO) and ν_s(COO) at 1670 and 1473 cm^{-1}, respectively, for the pure acid in Figure 4b give a frequency difference of 197 cm^{-1} fitting with the literature value of ≈200 cm^{-1} for the bridging geometry, as was shown by Jouet et al.[10] for perfluorotetradecanoic acid. As these peaks are not evident in spectra for untreated aluminum, we can deduce that the PFPA SAM on aluminum is bound via carboxylate bridging.

Once this coordination is confirmed, peak area measurements from the XPS C1s spectrum in Figure 3a can be used to evaluate the percentage of oxygen dedicated to COOH groups. This information is compared with the percentage of aluminum oxidized in the Al2p spectrum in Figure 3b. Resulting calculations show that of the percentage of the oxide peak attributed to functionalized aluminum is 56%. Thus, XPS has shown that not only is the coating layer, seen in TEM Figure 2a, much thinner than the untreated case, only 44% of the mass in that 1–2 nm coating is composed of Al_2O_3. In the gas-phase bonding between the carboxylic acid group and aluminum, the formation of a small percentage of aluminum oxide indicates that though we have prevented reaction to form a thick oxide layer, there is still a small percentage of available sites. Bridge bonding chains are not fully able to arrange preferentially on the aluminum surface in this gas-phase coating system. Since most of the aluminum is successfully bound to carboxylate groups, however, further penetration is successfully averted to avoid significant loss of core material.

Part. Part. Syst. Charact. **2013**,
DOI: 10.1002/ppsc.201300112

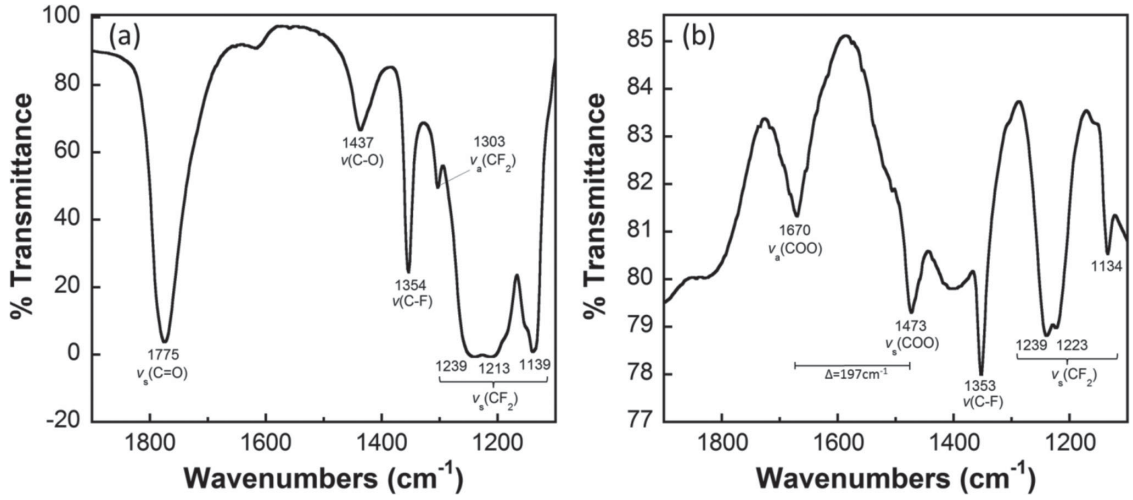

Figure 4. FTIR transmittance spectra for a) free PFPA acid and b)PFPA-coated Al.

The Cabrera–Mott model for oxidation of bare metal nanoparticles details the process to form the alumina layer.[22,23] Initial attachment of oxygen onto the metal surface creates an electric field between the oxide shell and the core, driving diffusion of metal ions outward and coming into contact with oxygen. Our results suggest that bonding with the carboxylate group on the fluorocarboxylic acid might alter this electric field and keep outward diffusion of aluminum ions at bay.

3.2. Reactivity Investigation

TGA tests were completed with precise measurement of sample weight gain while heating to 1200 °C, as shown in **Figure 5**. The increase in mass is attributed to complete oxidation of aluminum, and thus results allow for calculation of percentage of active aluminum in the original sample.

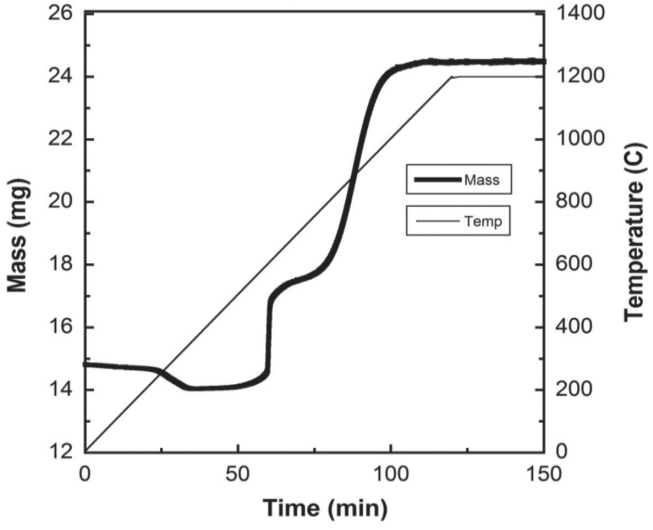

Figure 5. TGA experimental data for heating of PFPA-treated nanoaluminum.

Weight measurement results show an initial mass of 14.82 mg, a lowpoint mass of 14.04 mg after evaporation of adsorbed water and hydrocarbon contamination, and a final mass of 24.53 mg. The initial mass decrease is similar to a previously tested untreated aluminum case, indicating that this fluorocarbon coating does not cause any increase in water adsorption. The stall in the mass gain between temperatures of 600–700 °C indicates melting of aluminum metal consistent with previous testing.[19] The difference between the lowpoint and final mass values gives an active aluminum content of 80%, a significant increase compared with the untreated aluminum result of 63% shown previously.[19] This information is consistent with TEM and XPS results showing a much thinner coating layer for the PFPA-treated product. A calculation of theoretical active percentage for a 90-nm particle of bipyramidal shape with coating proportionate to XPS results shows a similar change in active percentage, 65% for uncoated and 83% for PFPA-coated aluminum.

Since low fuel percentage is one of the major industrial concerns regarding oxide formation, our 17% increase in active aluminum provides strong evidence for gas-phase PFPA coating as a practical method for passivation coating. Direct comparison with fuel percentages for commercial nanoaluminum, e.g., Argonide Corp. Al 70% active, average diameter ≈50 nm,[19] can be misleading due to significant variance in content with particle size, but nonetheless a ≈90 nm nanoaluminum product at 80% active content can clearly be regarded a valuable result for energetic purposes considering the lower proportions for our untreated samples.

Hot-wire ignition testing was accomplished for stoichiometric thermite (sample/CuO) combinations of untreated aluminum, PFPA-passivated aluminum, and aluminum sample allowed to form an oxide layer and subsequently coated with PFPA. High-speed video recorded throughout the event allows for visual confirmation of ignition at corresponding time values, as shown in **Figure 6**.

The coated aluminum in Figure 6a shows evidence of ignition considerably earlier than the untreated aluminum,

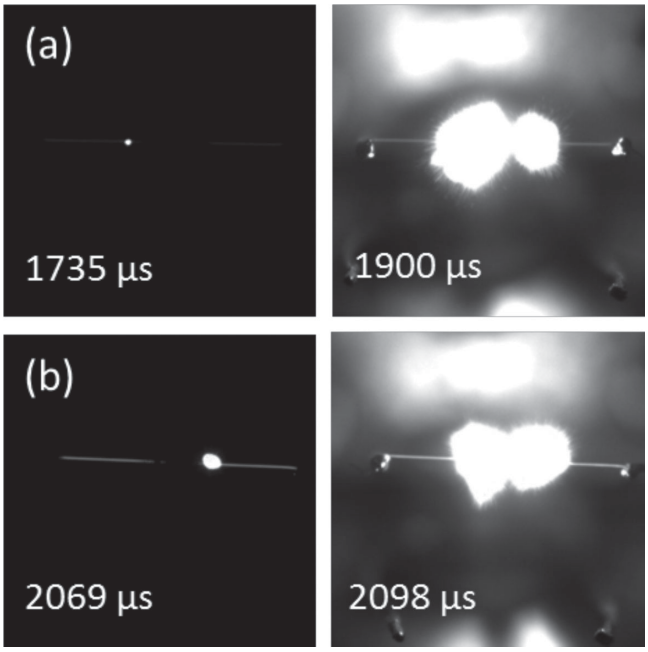

Figure 6. High-speed video of T-jump ignition experiments for a) PFPA-treated-Al/CuO and b) untreated-Al/CuO combinations. Note: same heating rate per pulse in each event.

suggesting energetic enhancement. To confirm and calculate critical ignition temperature, appropriate time measurements at the point of ignition are used in conjunction with wire resistance measurements as well as voltage and transient current through the circuit. For further comparison, a sample of aluminum was allowed to form a regular ≈4 nm oxide layer and was subsequently coated with PFPA. Calculated ignition temperatures averaging three runs with a heating pulse of ≈3 ms are shown in **Table 1** for the three thermite combinations.

Results show a significantly lower critical ignition temperature of ≈955 K for the PFPA-passivated Al thermite compared with ≈1057 K for the untreated aluminum thermite, consistent with high-speed video observations in Figure 6. The ignition temperature is also slightly lower for the coated sample with an aluminum oxide layer underneath, indicating a contribution of direct oxidizer delivery via PFPA coating for lowering of ignition temperature. This observation corresponds with results from Pantoya and Dean[18] detailing an exothermic preignition reaction between aluminum oxide and fluorine to form AlF_3 and exposing the particle core for reaction. Further decrease in ignition temperature for our passivated aluminum sample can be ascribed to the decreased thickness in the aluminum oxide layer. The small amount of Al_2O_3 present can react with fluorine and quickly expose the core to oxidize, whereas a thicker layer will require more time to fluorinate and reveal metallic Al. To probe for fluorinated aluminum in flame-ignited passivated sample, XPS is employed to evaluate chemical composition of reaction products, as shown in **Figure 7**.

Table 1. T-jump wire ignition results comparing Al, PFPA-passivated Al, and Al(with oxide layer)-PFPA-coated; all combined with stoichiometric CuO.

Sample	Ignition temperature [K]
Al/CuO	≈1057
PFPA-passivated-Al/CuO	≈955
Al(with oxide layer)-PFPA-coated/CuO	≈1003

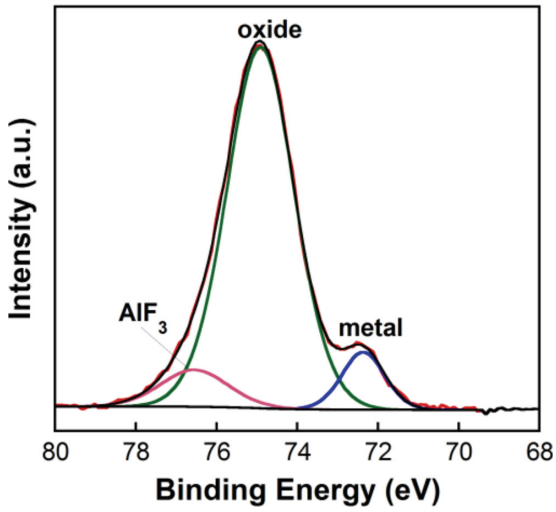

Figure 7. XPS Al2p spectrum for flame-ignited sample of PFPA-treated aluminum.

Formation of AlF_3 in the char product agrees with evidence from thin wire T-jump ignition tests proposing a fluorine–aluminum interaction contributing to decrease in critical ignition temperature. Whether this reaction has occurred between fluorine and core aluminum or substitution with Al_2O_3 by the preignition reaction[18] cannot be determined from these tests.

4. Conclusions

A gas-phase scheme for coating of bare nanoaluminum with PFPA is shown by TEM and XPS to protect from penetration of oxygen further than 1 to 2 nm. The coating is indicated by TGA to yield significant improvement in fuel percentage, a value of 80% active aluminum compared to 63% for the untreated case. XPS confirms the presence of the fluorocarboxylic acid, and FTIR analysis determines a bridging carboxylate bonding with the aluminum surface. Hot-wire temperature-jump ignition tests for thermite mixtures with CuO show a decreased critical ignition temperature for the PFPA-passivated aluminum thermite compared with untreated. Further testing shows a slight decrease in ignition temperature for oxide-passivated aluminum coated with PFPA, indicating contributions from the exothermic reaction for fluorination of aluminum during the combustion event. This theory is upheld by the presence of AlF_3 in XPS spectra for flame-ignited PFPA-passivated aluminum. Thus, we have produced a true functional passivation coating; a reduced critical ignition temperature is obtained by prevention of thick oxide layer formation and reaction during combustion with the fluorocarboxylic acid layer.

Part. Part. Syst. Charact. **2013**,
DOI: 10.1002/ppsc.201300112

Acknowledgements

Support for this work comes from the Defense Threat Reduction Agency, the Army Research Office, and the University of Maryland Center for Energetic Concepts Development (CECD). The authors also gratefully acknowledge the support of the Maryland NanoCenter and its NispLab. The NispLab is supported in part by the NSF as a MRSEC Shared Experimental Facility.

Received: March 4, 2013
Revised: May 22, 2013
Published online:

[1] D. G. Piercey, T. M. Klapotke,*Cent. Eur. J. Energ. Mater.* **2010**, *7*, 114.
[2] C. Rossi, A. Esteve, P. Vashishta, *J. Phys. Chem. Solids* **2010**, *71*, 57.
[3] C. Rossi, K. Zhang, D. Esteve, P. Alphonse, P. Tailhades, C. Vahlas, *J. Microelectromech. Syst.* **2007**, *16*, 919.
[4] R. A. Yetter, G. A. Risha, S. F. Son, *Proc. Combust. Inst.* **2009**, *32*, 1819.
[5] E. L. Dreizin, *Prog. Energy Combust. Sci.* **2009**, *35*, 141.
[6] D. S. Wen, *Energy Environ. Sci.* **2010**, *3*, 591.
[7] A. Rai, K. Park, L. Zhou, M. R. Zachariah, *Combust. Theor. Model* **2006**, *10*, 843.
[8] G. Jian, N. W. Piekel, M. R. Zachariah, *J. Phys. Chem. C* **2012**, *116*, 26881.
[9] D. W. Hammerstroem, M. A. Burgers, S. W. Chung, E. A. Guliants, C. E. Bunker, K. M. Wentz, S. E. Hayes, S. W. Buckner, P. A. Jelliss, *Inorg. Chem.* **2011**, *50*, 5054.
[10] R. J. Jouet, A. D. Warren, D. M. Rosenberg, V. J. Bellitto, K. Park, M. R. Zachariah, *Chem. Mater.* **2005**, *17*, 2987.
[11] R. J. Jouet, J. R. Carney, R. H. Granholm, H. W. Sandusky, A. D. Warren, *Mater. Sci. Technol.* **2006**, *22*, 422.
[12] B. Balasubramanian, K. L. Kraemer, N. A. Reding, R. Skomski, S. Ducharme, D. J. Sellmyer, *ACS Nano.* **2010**, *4*, 1893.
[13] L. Zhang, M. B. Ranade, J. W. J. Genry, *Aerosol Sci.* **2003**, *35*, 457.
[14] J. M. Horn, J. Lightstone, J. Carney, J. Jouet, *AIP Conf. Proc.* **2012**, *1426*, 607.
[15] K. S. Kappagantula, C. Farley, M. L. Pantoya, J. Horn, *J. Phys. Chem. C.* **2012**, *116*, 24469.
[16] C. A. Crouse, C. J. Pierce, J. E. Spowart, *Combust. Flame* **2012**, *159*, 3199.
[17] K. W. Watson, M. L. Pantoya, V. I. Levitas, *Combust. Flame* **2008**, *155*, 619.
[18] M. L. Pantoya, S. W. Dean, *Thermochim. Acta* **2009**, *493*, 109.
[19] D. A. Kaplowitz, R. J. Jouet, M. R. Zachariah, *J. Cryst. Growth* **2010**, *312*, 3625.
[20] L. Zhou, N. Piekiel, S. Chowdhury, M. R. Zachariah, *Rapid Commun. Mass Spectrom.* **2009**, *23*, 194.
[21] J. Mihaly, S. Sterkel, H. M. Ortner, L. Kocsis, L. Hajba, E. Furdyga, J. Mink, *Croat. Chem. Acta* **2006**, *79*, 497.
[22] N. Cabrera, N. F. Mott, *Rep. Prog. Phys.* **1948**, *12*, 163.
[23] V. P. Zhdanov, B. Kasemo, *Chem. Phys. Lett.* **2008**, *452*, 285.